International Journal of Heat and Mass Transfer 52 (2009) 3576–3584

Contents lists available at ScienceDirect

International Journal of Heat and Mass Transfer

journal homepage: www.elsevier.com/locate/ijhmt

Dynamical and thermal performance of molten salt pipe during filling process

Lu Jianfeng, Ding Jing *

School of Engineering, Sun Yat-Sen University, Guangzhou 510006, China

ARTICLE INFO

Article history:
Received 27 June 2008
Received in revised form 24 February 2009
Accepted 2 March 2009
Available online 16 April 2009

Keywords:
Molten salt
Filling process
Heat transfer
Freeze
VOF

ABSTRACT

The dynamical and thermal performances of molten salt pipe during the filling process are numerically investigated using volume of fluid model. The whole filling process has three main stages, or the developing stage with the interface width quickly increasing, the fluctuating stage with the interface width fluctuating and the fully developed stage with stable interface, and then associated interface structures, flow and temperature fields are described in detail. Before the molten salt flows through a certain position, the fluid temperature will jump within a short time, while the wall temperature only linearly increases after that. The heat transport during the filling process is mainly dependent upon the pipe wall and molten salt flow, while natural convection outside can almost be ignored. The dimensionless interface temperature has similar evolution process under different surrounding temperatures, but it will apparently increase with the flow velocity rising. In addition, the pipe will be blocked when the interface temperature drops below the freezing point, so a model of penetration distance is derived by correlating the interface temperature evolution process, and it has a good agreement with available experimental results.

1. Introduction

In modern society, the energy resource shortage and environmental pollution have become critical problems, so there is an urgent demand for clean and renewable energy. Since the renewable energy, as solar or biology energies, has the characteristics of dispersity and discontinuity, the thermal energy storage is an important technology. Recently, the molten salts at high temperature have been widely employed to improve the heat transfer performance of thermal storage devices and/or meet the increasing demand of high heat removal and storage in aerospace science and technology [1], solar thermal power [2,3], and other industrial applications. The molten salts have many advantages including large thermal capacity, high chemical stability, low viscosity and a wide range of operating temperature, and it has been proposed as a suitable medium for thermal storage and cycle fluid at high temperature.

The filling process is an important problem in the startup stage of molten salt system, and it has many scientific topics of flow dynamics, heat transfer, and phase change phenomena. Since the freezing point of molten inorganic salts is usually not high enough, the molten salt freezing phenomenon is a serious problem. In the startup stage of the molten salt system, the molten salt probably freezes when it flows along the cold pipe. Pacheco et al. [4] investigated cold fill experiments by flowing molten salt through cold panels, and the transient thermal responses and penetration distance were also measured. Pacheco and Dunkin [5] further considered the effects of a molten salt receiver freeze-up and recovery event. Available literature has presented experimental results and associated analyses about the molten salt freezing phenomena, but few researchers have conducted theoretical analyses and numerical simulation on the basic dynamical and thermal performance of the molten salt filling process.

The filling process is mainly a multiphase flow process as the molten salt replacing the air in the pipe system. As a transient process, it is not easy to measure the local dynamical and thermal parameters in detail, so the numerical method can benefit the investigation. In last decade, numerical method is increasing and widely developed to investigate the multiphase flow. A series of numerical methods was proposed to simulate the phase boundary in various problems, as VOF (volume of fluid) [6,7], CIP (the constrained interpolation profile) [8] and phase field method [9]. Tseng et al. [10] calculated the fluid filling into micro-fabricated reservoirs by VOF and CSF (continuum surface force model). Alexandrou et al. [11] studied the Bingham fluid filling of a 2D cavity using PAM-CAST/SIMULOR, which was modified by introducing a regularized Bingham fluid constitutive relation, and then identified five different flow patterns. Shin and Lee [12] proposed a modified volume of fluid method based on four node elements in 2D geometry for its compatibility with the irregular meshes, and the mold filling process was studied to demonstrate the effectiveness of the proposed numerical scheme. Katzarov [13] used the finite element method to simulate 3D form filling process with

* Corresponding author. Tel.: +86 10 39332320; fax: +86 10 39332319.
E-mail address: liujf01@mails.tsinghua.edu.cn (J. Lu).

0017-9310/$ - see front matter © 2009 Elsevier Ltd. All rights reserved.
doi:10.1016/j.ijheatmasstransfer.2009.03.005

Nomenclature

c	thermal capacity ($J\,kg^{-1}\,K^{-1}$)
E	apparent energy ($J\,kg^{-1}$)
g	gravity acceleration ($m\,s^{-2}$)
H	thickness (m)
h	heat transfer coefficient ($W\,m^{-2}\,K^{-1}$)
P	pressure (Pa)
q	heat flux ($W\,m^{-2}$)
R_1	inner pipe radius (m)
R_2	outer pipe radius (m)
S	mass source due to phase change ($kg\,s^{-1}\,m^{-3}$)
T	temperature (K)
t	time (s)
u	velocity ($m\,s^{-1}$)
v	velocity ($m\,s^{-1}$)
W	interface width (m)
x, y, z	coordinate (m)

Greek symbols

α	volume fraction (–)
ρ	density ($kg\,m^{-3}$)
λ	thermal conductivity ($W\,m^{-1}\,K^{-1}$)
θ	dimensionless temperature (–)
μ	viscosity ($kg\,m^{-1}\,s^{-1}$)

Subscripts

0	inlet condition, initial condition
g	gas phase
l	liquid phase
s	solid phase, surrounding condition
i	interface

incompressible fluid. In addition, the molten salt filling process and associated heat transfer characteristics need further investigation using the numerical method.

This paper mainly presents numerical simulations and analyses on the dynamical and thermal performance of molten salt pipe during filling process. The filling process is simulated using volume of fluid model (VOF) and the standard k–ε model. The basic interface structures, flow and temperature fields of molten salt system are presented during the whole filling process, and the characteristics of the temperature evolution and heat flux distribution are further described. In order to consider the freezing phenomena during filling process, the interface temperature evolution characteristics are studied under different surrounding temperatures and flow velocities, and then the penetration distance model of the molten salt is also proposed.

2. Physical and mathematical description

2.1. Basic physical model

In order to demonstrate the filling process of molten salt in a straight pipe in detail, a Cartesian coordinate system is established in Fig. 1. The inner and outer radii of the pipe made of steel are R_1 and R_2 or 0.008 m and 0.010 m, respectively, while its length is 5 m. The heat transfer coefficient outside the pipe is h with the surrounding temperature T_s, and the gravity acceleration g is 9.8 $m\,s^{-2}$.

In many heat storage systems, a widely used medium is HITEC heat transfer salt composed of potassium nitrate, sodium nitrite, and sodium nitrate. The properties of the molten salt [14], air and steel [15] are assumed constant except the viscosity of the molten salt, as illustrated in Table 1. The freezing point T_f and latent heat of molten salt h_{sl} are, respectively, 413 K and 59 $kJ\,kg^{-1}$. During the filling process of molten salt in the pipe, the velocity is 1–3 m/s, and the Reynolds number is about 6000–18,000, so

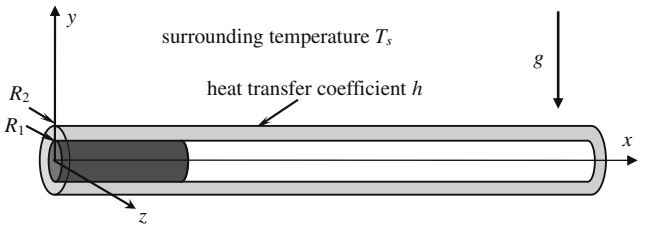

Fig. 1. The basic physical model of the filling process.

Table 1
Properties of molten salt, air and steel in present simulation.

Molten salt		Air		Steel	
ρ_l	1940 $kg\,m^{-3}$	ρ_g	1.225 $kg\,m^{-3}$	ρ_s	8030 $kg^{-1}\,m^{-3}$
c_l	1510 $J\,kg^{-1}\,K^{-1}$	c_g	1006 $J\,kg^{-1}\,K^{-1}$	c_s	502.48 $J\,kg^{-1}\,K^{-1}$
λ_l	0.571 $W\,m^{-1}\,K^{-1}$	λ_g	0.0242 $W\,m^{-1}\,K^{-1}$	λ_s	16.27 $W\,m^{-1}\,K^{-1}$
μ_l	$-0.000021T+$ 0.0154 $kg\,m^{-1}\,s^{-1}$	μ_g	0.000017854 $kg\,m^{-1}\,s^{-1}$		

the standard k–ε model is adopted to analyze the filling process in this simulation.

2.2. Governing equation

The filling process in present article will be numerically investigated using volume of fluid model (VOF). In VOF model, the information on phase distribution can be directly extracted from the volume fractions, and volume fractions of all phases sum to unity:

$$\alpha_l + \alpha_g = 1 \tag{1}$$

where the primary phase is air with volume fraction α_g, and the secondary phase is molten salt with volume fraction α_l. At initial time, α_l reaches the minimum value of 0, and it will increase to the maximum value of 1 as the filling process going on. At the phase interface, α_l and α_g varies between 0 and 1.

The tracking of the interface between the two phases can be accomplished by the solution of continuity equations for the volume fraction of two phases. For the liquid and gas phases, the equations are:

$$\frac{\partial \alpha_l}{\partial t} + \overline{v}\nabla\alpha_l = \frac{S_l}{\rho_l} \tag{2a}$$

$$\frac{\partial \alpha_g}{\partial t} + \overline{v}\nabla\alpha_g = \frac{S_g}{\rho_l} \tag{2b}$$

In present investigation, $S_l = S_g = 0$.

The momentum equation including the gravity acceleration effect is

$$\frac{\partial(\rho\overline{v})}{\partial t} + \nabla(\rho\overline{v}\overline{v}) = -\nabla p + \nabla\left[\mu(\nabla\overline{v} + \nabla\overline{v}^T)\right] + \rho g \cdot j \tag{3}$$

where j denotes vertical direction y.

The energy equation can be described as:

$$\frac{\partial(\rho E)}{\partial t} + \nabla[\overline{v}(\rho E + p)] = \nabla\cdot(k\nabla T) + Q \tag{4}$$

where

$$\rho = \alpha_l\rho_l + \alpha_g\rho_g, \quad k = \alpha_l k_l + \alpha_g k_g, \quad \mu = \alpha_l\mu_l + \alpha_g\mu_g,$$
$$E = \frac{\alpha_l\rho_l E_l + \alpha_g\rho_g E_g}{\alpha_l\rho_l + \alpha_g\rho_g}$$

The governing equation in the solid zone (steel) is given as:

$$\rho_s c_s \frac{\partial T}{\partial t} = \lambda_s \nabla^2 T \tag{5}$$

The properties of the steel are assumed constant as shown in Table 1.

Additionally, the boundary conditions of the fluid zone at inlet and outlet are, respectively, inlet velocity of u_0 and outflow, while the boundary conditions of the pipe wall at inlet and outlet are, respectively, isothermal of temperature T_0 and isoflux of zero.

2.3. Mesh construction and simulation procedure

The computational domain including the fluid and solid zone is strictly half of Fig. 1 with symmetry condition. The computational mesh of the pipe and wall volume is comprised by 67,600 hexahedral volume elements, and the grid number on the cross-section of the pipe is about 340. Calculations with about 200,000 or 30,000 elements yield similar results, in terms of the velocity and temperature distributions, to those described here.

Since there is a great difference between the densities of air and molten salt, the Pressure-Implicit with Splitting of Operators (PISO) pressure–velocity coupling scheme is accomplished to derive the approximate relation between the corrections for pressure and velocity. The PISO has two additional corrections of neighbor correction and skewness correction, which help to improve the efficiency of calculation. Upwind scheme of second order accuracy is adopted to discretize the momentum and energy equations. In present simulations, the residual errors of velocity and energy are smaller than 10^{-5}.

The whole simulation procedure has two steps: the steady process before the filling process, and the filling process. Before the filling process, the pipe acts as a long fin with inlet boundary temperature T_0. Fig. 2 illustrates the initial temperature distribution of the pipe wall, and the surrounding temperature T_s can significantly affect the initial temperature distribution, while the heat transfer coefficient h only has little effect. During the filling process, the molten salt will be pumped into the pipe with velocity u_0, and then the dynamical and thermal characteristics of molten salt pipe can be investigated using VOF model.

3. Evolution phenomena during the molten salt filling process

3.1. General description

Since various simulation results indicate that the basic dynamic and heat transfer performances of molten salt filling processes are similar, a specified example will be further investigated with the surrounding temperature 300 K, inlet velocity $u_0 = 1$ m/s, and heat transfer coefficient $h = 10\ \mathrm{W\,m^{-2}\,K^{-1}}$.

The interface of molten salt on the symmetry plane ($z = 0$) is typically illustrated in Fig. 3. Obviously, the maximum height of the interface in vertical direction is equal to the inner diameter of the pipe or $2R_1$. Because of the gravity acceleration, the interface expands in the horizontal direction and its length is usually remarkably larger than its height. In the vertical section A–A, the interface adjacent to pipe wall is a little higher than the middle region because of the interface tension.

For a quantitative investigation, the interface can be described with its geometrical parameter of width, W, as illustrated in Fig. 3. The evolution of interface width during the filling process is illustrated in Fig. 4, and it mainly has three stages. Before 0.40 s, the interface width increases sharply from zero to 0.18 m, and this stage can be named as stage I or the developing stage. In stage II or during 0.40–3.0 s, the interface width varies between 0.18 and 0.25 m like a weakening oscillation process, and this is the fluctuating stage. After 3.0 s, the interface width keeps constant, and the flow dynamic process is also stable, so stage III is a fully developed stage.

3.2. Developing stage

During the developing stage, the interface structure and associated flow and temperature distributions on the vertical plane ($z = 0$) can be illustrated in Fig. 5. At the first 0.05 s, the interface is almost symmetry, and two corners controlled by the pipe wall appear in the front of the interface. At 0.10 s, the interface width expands from 0.01m to 0.035 m, and the lower corner moves much more quickly than the upper one for the gravity effect. At 0.15 s, the upper corner disappears, and the front of the interface becomes a tip. As a result, the basic interface structure forms with one tip near the lower wall. At 0.30 s, the interface keeps its basic structure, but its width expands evidently.

Additionally, the flow and temperature distributions will be considered in detail. At 0.05 s, the velocity near the interface is very uniform except the boundary layer, and the maximum velocity 1.33 m/s appears in front of the interface. During 0.10–0.15 s, the velocity of the interface near the lower wall increases because the gravity drives the interface expanse near the tip, and the

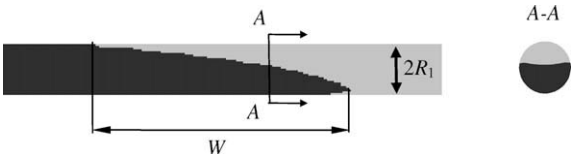

Fig. 3. The basic interface structure.

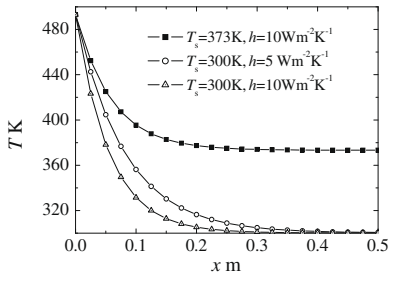

Fig. 2. The initial temperature distribution of the pipe.

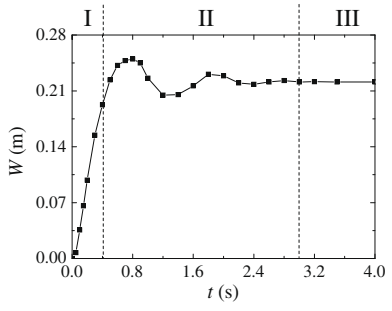

Fig. 4. The evolution of the interface width.

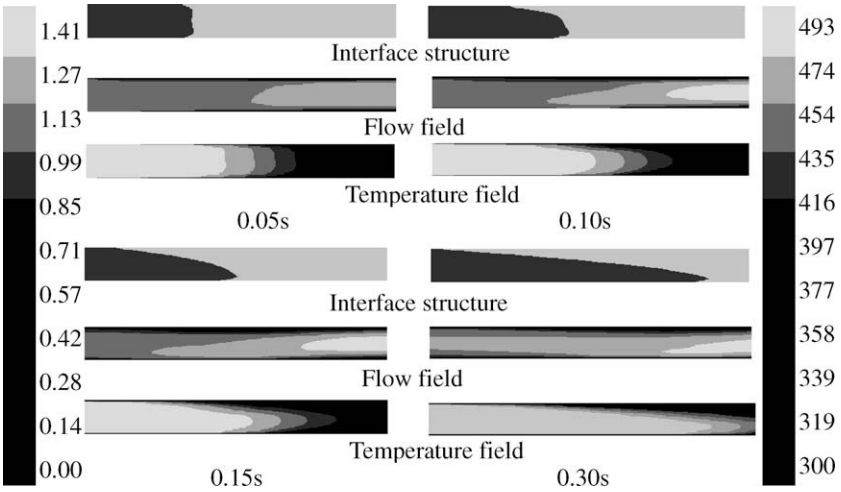

Fig. 5. The interface structure and associated flow and temperature distributions on vertical plane ($z = 0$) during the developing stage.

maximum flow velocity reaches 1.41 m/s. At 0.30 s, the flow boundary layer remarkably develops, and the maximum velocity exists near the interface tip. Generally, the velocity distributes like a tip, but its direction is just opposite to that of interface. Since the thermal conductivity of the molten salt is much higher than that of air, the temperature varies very sharply near the interface and the temperature distribution is similar to that of interface structure. Before 0.10 s, the temperature distribution is almost symmetry, and after that there appears a temperature tip near the lower wall.

The temperature and flow distributions in several cross-sections A–C are investigated in Fig. 6. In the end of the interface or section A, the velocity in x direction is almost axial symmetry with maximum velocity in the center and a very thin boundary layer, and the velocity in y–z plane is very little, consequently the temperature is almost axial symmetry. In the middle of the interface or section B, the maximum velocity in x direction appears near the lower wall, and the two eddies in y–z plane remarkably develops. Besides, the flow and thermal boundary layers obviously develop near the upper wall. In the front of the interface or section C, the flow region with high velocity expands, and the velocity in y–z plane is similar to that in section B. Generally, the temperature distributions in the cross-sections are similar to the flow distribution.

3.3. Fluctuating stage

Fig. 7 illustrates the interface structure and associated flow and temperature distributions on vertical plane ($z = 0$) during the fluctuating stage. From 0.8 s to 1.2 s, the interface keeps its basic structure, but its width shrinks from 0.250 m to 0.205 m. Because of the interface shrinkage, the velocity adjacent to the lower wall will be smaller than that near the upper wall. As a result, the tip of the velocity distribution appears near the upper wall, and this is quite different from the phenomenon in the developing stage. Besides, the temperature distribution is still similar to the interface structure, but it decreases very obviously as the time going on. During 0.8–1.2 s, the interface temperature at the pipe axis significantly decreases from 478 K to 454 K, while the maximum velocity slowly decreases from 1.41 m/s to 1.40 m/s.

3.4. Fully developed stage

During the fully developed stage, the interface structure and associated flow and temperature distributions on vertical plane ($z = 0$) is illustrated in Fig. 8. The fully developed interface is like a flat plane with width of 0.22 m, and there is only a small angle between the horizontal direction and interface because the gravity and inertia effects. In general, the bulk velocity of the air flow is higher than that of the molten salt flow. In the end of the interface or section A, the flow boundary layer near the upper wall is obviously thinner than that near the lower wall, and the velocity in y–z plane can almost be ignored. In the front of the interface or section B, the boundary layer near the upper wall obviously develops, and the two eddies in y–z plane develops. In addition, the temperature distribution is still similar to the interface structure.

For a quantitative investigation, the velocity and temperature distributions at the interface (the intersection of the interface and vertical plane $z = 0$) during the fully developed stage are described in Fig. 9. Generally, the interface velocity in the bulk flow region is 1.21 m/s, and the thickness of flow boundary layer is about 0.003 m. The interface temperature in the bulk flow region is 422 K, which is only 9 K higher than the freezing point, and the thermal boundary layer is just similar to the flow boundary layer. Meanwhile, the temperatures of the upper and lower walls are only 303.1 K and 300.8 K, so the molten salt will probably freeze near the wall. Since the interface temperature in the bulk region has little variation, it can be assumed as the characteristic interface temperature T_i.

4. Basic thermal characteristics of the filling process

4.1. The temperature distributions of the fluid and wall

Fig. 10 illustrates the temperature distributions of the wall and bulk flow along x direction, where the fluid, upper wall and lower wall denote $y = 0$ m, 0.009 m, − 0.009 m with $z = 0$, respectively.

At 0.500 s, the molten salt with the average velocity 1 m/s mainly inhabits the region between 0 m and 0.5 m, while the region beyond 0.5 m is still filled with air. In the molten salt region, the fluid temperature drops slowly from 493 K to 486.4 K, while the temperature in the air region quickly drops from 486.4 K to 300.5 K within 0.5–0.9 m. Corresponding to Fig. 2, the wall temperature distributes very similar to the initial temperature, and it drops from 493 K to 315 K within 0.2 m near the inlet. In addition, the upper wall is a little colder than the lower wall because the molten salt region near the lower wall is larger due to the interface structure.

At 3.000 s, the bulk fluid temperature in the molten salt region decreases gradually from 493 K to 423 K, while the temperature in the air region drops quickly from 423 K to 300.7 K in a very short

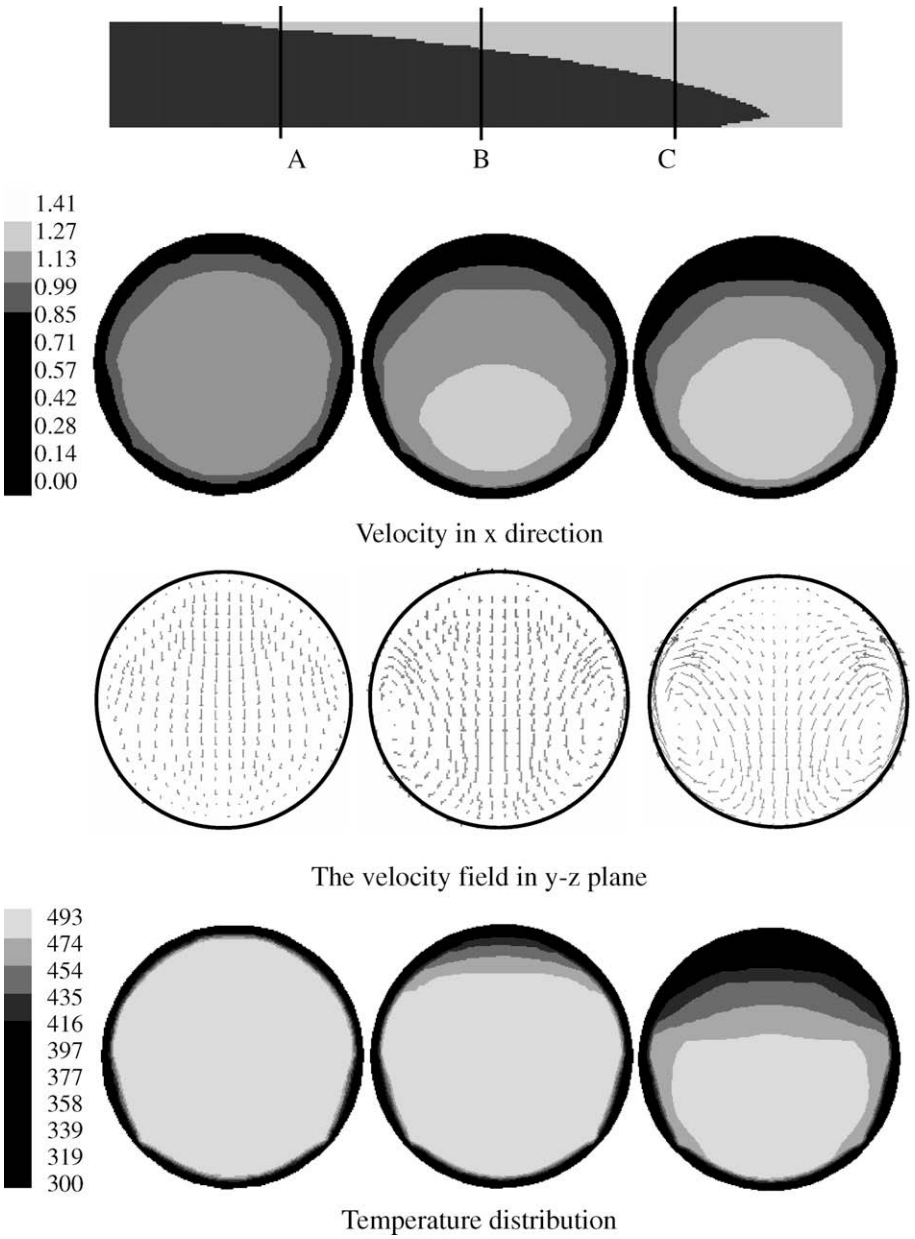

Fig. 6. The flow and temperature distributions at the cross-section at 0.20 s.

distance. The wall temperature distribution has three main regions. In the region near the inlet, the temperature decreases quickly from 493 K to 364.7 K within 0.2 m, and it is mainly dependent upon the inlet boundary effect. In the air region, the temperature is just near the surrounding temperature 300 K beyond 3.0 m, because the energy has not been transferred to this region through molten salt. In the molten salt region far from the inlet, the wall temperature linearly drops from 364.7 K to 300.4 K within the interval 0.2–3.0 m, and it is dependent upon the heating time.

4.2. The temperature evolution

Fig. 11 presents the wall and fluid temperature variations at special positions $x = 0.5$ m and 2.0 m. Apparently, the wall temperature evolution process has two main stages. Before the molten salt flows along the position, the wall temperature just keeps near the surrounding temperature. After the molten salt flows along the position, the wall temperature increases linearly because the wall is heated by the molten salt flow with high temperature. On the other hand, the fluid temperature evolution process can be divided into three stages. Before the molten salt flows along the position, the fluid temperature jumps from the surrounding temperature 300 K to the main fluid temperature within about 0.5 s. During a short time about 0.5 s after the molten salt flows along the position, the fluid temperature drops a little because the fluid is suddenly cooled by the cold wall. After that, the fluid temperature slowly increases with the wall temperature rising.

Fig. 12 illustrates the wall and fluid temperature distributions at different time, and their evolution processes are apparently very regular. In Fig. 12a, the wall temperature increases about 10 K within 0.5 s. As illustrated in Fig. 12b, the fluid temperatures in the molten salt region only have very little difference, and the basic temperature decreasing characteristics in the air region are also very similar. The main difference is that the temperature of the interface between the molten salt and air region drops as the time going on.

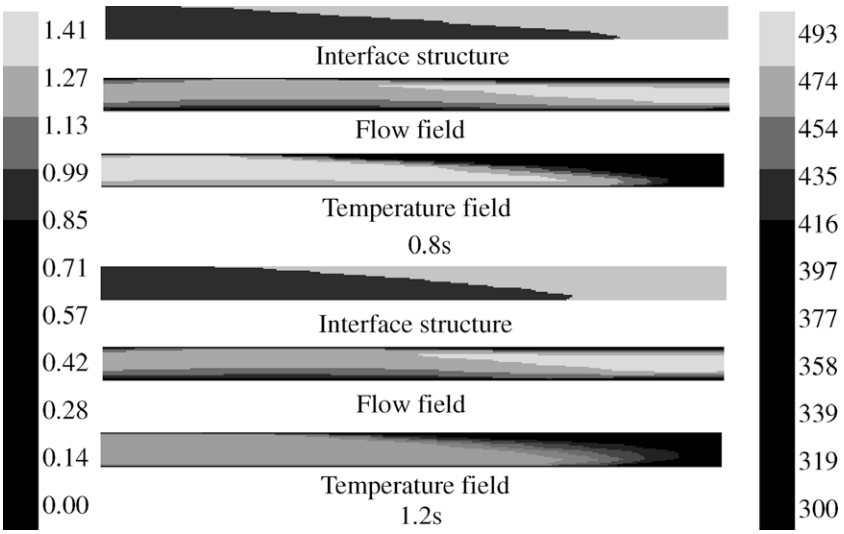

Fig. 7. The interface structure and associated flow and temperature distributions on vertical plane ($z = 0$) during fluctuating stage.

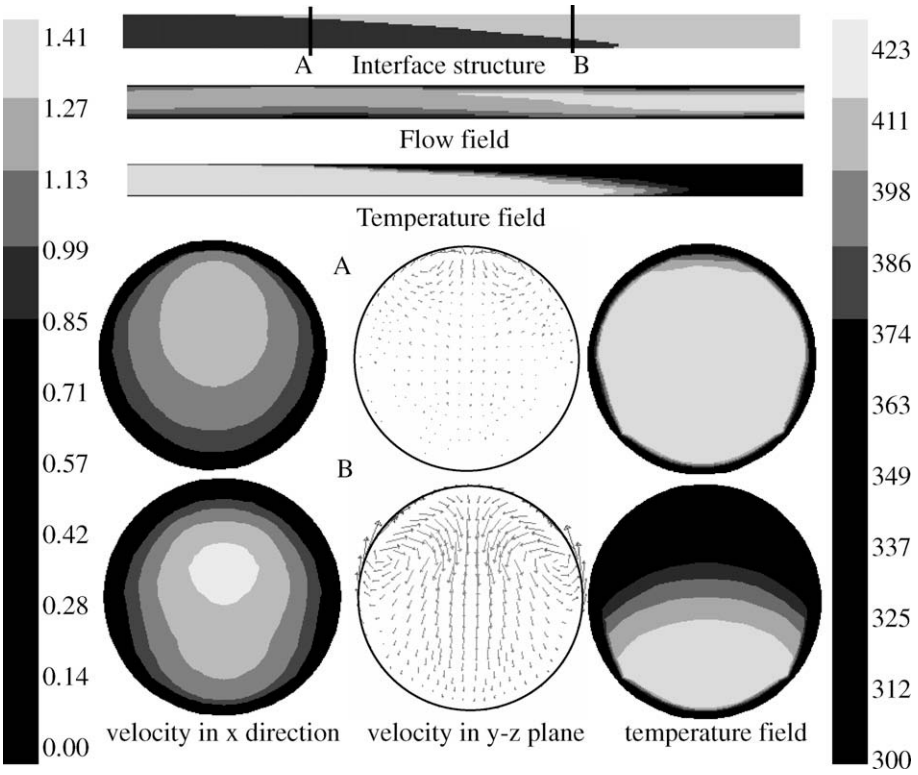

Fig. 8. The interface structure and associated flow and temperature distributions during fully developed stage on vertical plane ($z = 0$) and cross-sections at $t = 3.0$ s.

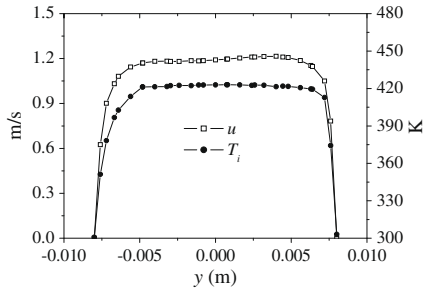

Fig. 9. The temperature and flow distributions at interface ($t = 3.0$ s).

4.3. The heat flux and heat transfer characteristics

Fig. 13 illustrates the heat flux of the outer pipe boundary q_{out} and inner boundary q_{in} along x direction. The heat flux of the outer boundary is caused by the natural convection, and it normally has direct ratio with the difference between the surrounding and wall temperatures. On the other hand, the heat flux of the inner boundary is dependent upon the natural convection and the wall internal energy increment. At 0.500 s, the heat flux of the outer boundary decreases from 1680 W m^{-2} to zero along x direction, while the heat flux of the inner boundary has several stages. Before 0.14 m, the heat flux of the inner boundary jumps from 23,200 W m^{-2} to

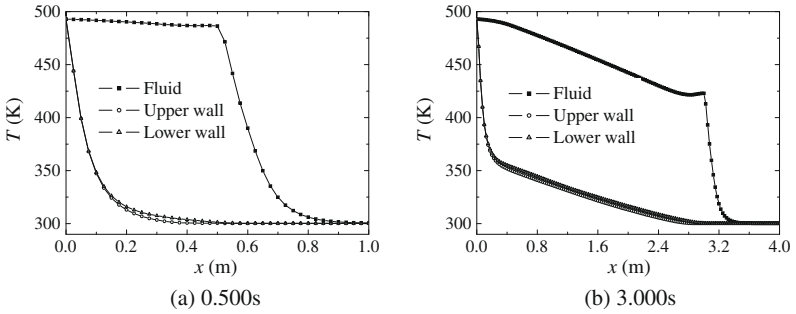

Fig. 10. The temperature distributions of the wall and fluid.

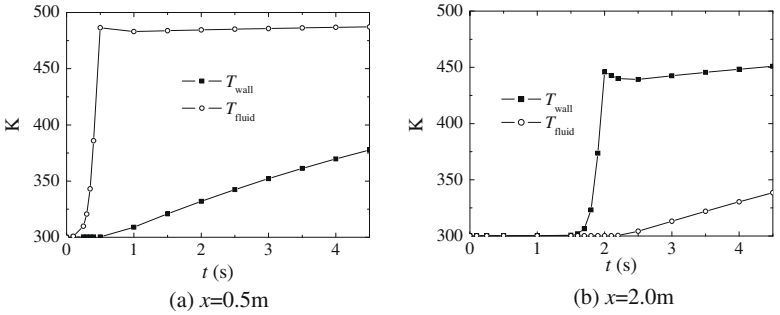

Fig. 11. The temperature variations at special positions.

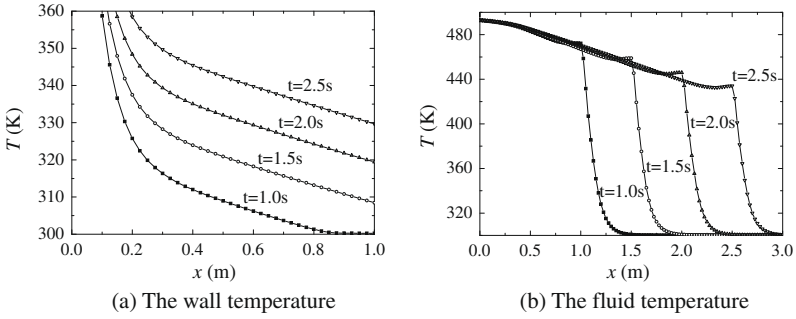

Fig. 12. The temperature distributions at different time.

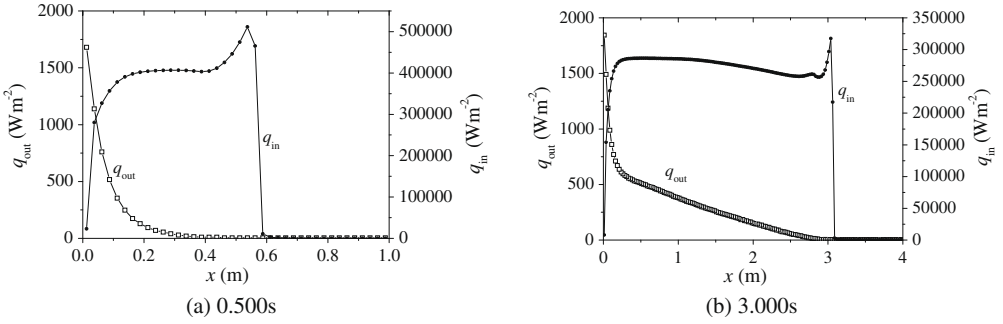

Fig. 13. The heat flux distributions of the outer and inner pipe boundary.

390, 500 W m^{-2}, and then it varies between 390, 500 W m^{-2}and 425, 500 W m^{-2} in the interval 0.14–0.54 m. In the interface region, the heat flux will reach its maximum 511, 300 W m^{-2}, and then it will finally drop to zero in the air region. At 3.000 s, the heat flux of outer boundary is similar to that at 0.500 s, while the heat flux of inner boundary has different distribution and it obviously drops in the interval 0.5–2.6 m.

According to Fig. 13, the heat flux of the outer boundary is only about 1% that of the inner boundary, so the thermal performance of the pipe wall determines the heat transfer process

during the filling process, and the natural convection outside can be ignored.

5. Blockage characteristics during the filling process

5.1. Interface temperature evolution

During the filling process, the pipe blockage caused by molten salt freezing phenomena is a serious problem, and it probably happens when the characteristic interface temperature T_i in Fig. 9 decreases to the freezing point.

Fig. 14a illustrates the characteristic interface temperature evolution under different surrounding temperatures, and they have two main stages. Before 0.5 s, the wall temperature obviously decreases near the inlet region as Fig. 10, and the heat flux between the wall and fluid near the interface increase, so the interface temperature decreasing rate will also rise. After 0.5 s, the wall temperature near the interface has little variation and the fluid temperature decreases, then the heat flux between the wall and fluid increases, and consequently the interface temperature drops with the decreasing rate gradually dropping. In addition, the evolution processes of the dimensionless interface temperature $\theta = (T_i - T_s)/(T_0 - T_s)$ can be described in Fig. 14b. Apparently, the interface temperature evolution processes are just similar under different surrounding temperatures, so the increment of surrounding temperature can directly increase the interface temperature.

Fig. 15 illustrates the characteristic interface temperature evolution process with different velocities. The evolution process still has two main stages, or the first stage with the interface temperature decreasing rate rising before 0.5 s, and the secondary stage with the temperature decreasing rate dropping after 0.5 s. Generally, the interface temperature will also increases as the velocity rising.

In practical system, in order to increase the characteristic interface temperature, the surrounding temperature can be increased by apply heat generation or steam tracing, and the velocity can be intensified by the pump power rising.

5.2. Penetration distance model

The penetration distance denotes the length of the region where the salt can flow in cold pipe prior to freezing closed, and it is mainly dependent upon the interface temperature evolution characteristics under different conditions.

From Fig. 14b, the dimensionless interface temperature θ almost linearly decreases with time going on, and can be modeled as:

$$\theta = \frac{T_i - T_s}{T_0 - T_s} = 1 - k \cdot t \tag{6}$$

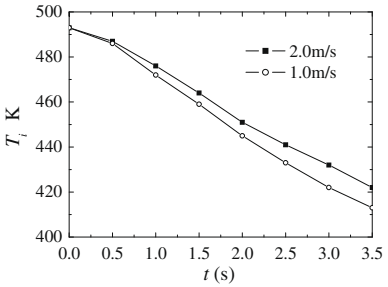

Fig. 15. The characteristic interface temperature with different velocities.

As a filling process, the interface position has direct relation with the time as $L_i = u_0 \cdot t$, and Eq. (6) will be:

$$\frac{T_i - T_s}{T_0 - T_s} = 1 - \frac{k}{u_0} \cdot x \tag{7}$$

When the interface freezes and the pipe is closed, the interface temperature is the freezing point T_f, and the penetration distance from Eq. (7) is

$$L_p = \frac{u_0}{k} \cdot \frac{T_0 - T_f}{T_0 - T_s} = K(u_0) \cdot \frac{T_0 - T_f}{T_0 - T_s} \tag{8}$$

where $K(u_0)$ is only dependent upon the fluid velocity and the molten salt system.

Bergan [16] reported the molten salt electric experiments of a receiver that was started cold. Pacheco et al. [4] studied the filling process by flowing the molten salt through cold panels, and summarized the data of penetration distance, as illustrated in Table 2. Calculate the parameter K from Eq. (8) with T_w, T_0, L_p in Table 2 and $T_f = 221\ ^\circ\mathrm{C}$, and K has a good consistency under different conditions. In practical system, the latent heat during the freezing process can delay the point where the tube is closed, and the penetration distance will be a little large than the simulated value here, but this does not affect the universality of this penetration distance model with the effects of inlet and surrounding conditions.

Table 2
Experimental and theoretical results of penetration distance.

T_s (°C)	T_0 (°C)	L_p (m)	K (−)
163	371	5.8	0.1243
116	343	4.2	0.1280
99	371	4.5	0.1225

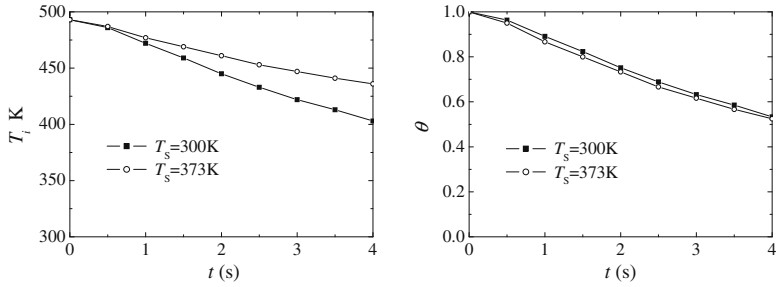

(a) Temperature variation (b) Dimensionless temperature variation

Fig. 14. The characteristic interface temperature variation.

6. Conclusions

In this investigation, the dynamical and thermal performances of the molten salt filling process are numerically investigated using volume of fluid model. According to the interface structure variation, the whole filling process mainly has three stages, or the developing stage with the interface width quickly increasing, the fluctuating stage with the interface fluctuating, and the fully developed stage with stable interface. Before the molten salt flows along a certain position, the wall temperature keeps near the surrounding temperature, while the fluid temperature will jump within a short time. After the molten salt passes through the local position, the wall temperature will increase linearly as time going on, while the fluid temperature changes very slowly. During the filling process, the inner energy increment of the pipe wall determines the heat transfer process, while the natural convection outside can be ignored.

The dimensionless interface temperature evolution processes are similar under different surrounding temperatures, while the increment of velocity can benefit the increasing of interface temperature. When the characteristic interface temperature is below the freezing point, the pipe will be blocked, and the penetration distance denotes the length of the region where the salt can flow. According to the interface temperature evolution process, the penetration distance is modeled, and it has a good agreement with available results.

Acknowledgement

This paper is supported by National Natural Science Foundation of China (No. 50806084) and China Postdoctoral Science Foundation (No. 20080430803).

References

[1] K.O. Lund, Heat rejection in thermal energy storage experiments for solar-dynamic space power development, in: ASME-JSES-JSME International Solar Energy Conference, 1991, pp. 387–398.
[2] U. Herrmann, B. Kelly, H. Price, Two-tank molten salt storage for parabolic trough solar power plants, Energy 29 (2004) 883–893.
[3] L. Moens, D.M. Blake, D.L. Rudnicki, M.J. Hale, Advanced thermal storage fluids for solar parabolic trough systems, ASME J. Solar Energy Eng. 125 (2003) 112–116.
[4] J.E. Pacheco, M.E. Ralph, J.M. Chavez, Investigation of cold filling receiver panels and piping in molten-nitrate-salt central-receiver solar power plants, J. Solar Energy Eng. Trans. ASME 117 (1995) 282–289.
[5] J.E. Pacheco, S.R. Dunkin, Assessment of molten-salt solar central-receiver freeze-up and recovery events, in: International Solar Energy Conference, 1996, pp. 85–90.
[6] C.W. Hirt, B.D. Nichols, Volume of fluid (VOF) method for the dynamics of free boundaries, J. Comput. Phys. 39 (1981) 201–225.
[7] R. Scardovelli, S. Zaleski, Direct numerical simulation of free-surface and interfacial flow, Annu. Rev. Fluid Mech. 31 (1999) 567–603.
[8] T. Utsumi, T. Yabe, T. Aoki, J. Koga, M. Yamagiwa, Solutions of hyperbolic equations with the CIP-BS method, JSME Int. J. B Fluids Therm. Eng. 47 (2004) 768–776.
[9] D. Jacqmin, Calculation of two-phase Navier–Stokes flows using phase-field modeling, J. Comput. Phys. 155 (1999) 96–127.
[10] F.G. Tseng, I.D. Yang, K.H. Lin, K.T. Ma, M.C. Lu, Y.T. Tseng, C.C. Chieng, Fluid filling into micro-fabricated reservoirs, Sens. Actuat. A 98 (2002) 131–138.
[11] A.N. Alexandrou, E. Duc, V. Entov, Inertial, viscous and yield stress effects in Bingham fluid filling of a 2-D cavity, J. Non-Newton. Fluid Mech. 96 (2001) 383–403.
[12] S. Shin, W. Lee II, Finite element analysis of incompressible viscous flow with moving free surface by selective volume of fluid method, Int. J. Heat Fluid Flow 21 (2000) 197–206.
[13] I.H. Katzarov, Finite element method for simulation of 3-D form filling with incompressible fluid, Int. J. Heat Mass Transfer 42 (1999) 3331–3336.
[14] E.I. du Pont de Nemours & Company, Hitec heat transfer salt, Inc., Explosives Dept., Bulletin.
[15] J.H. Lienhard IV, J.H. Lienhard V, A Heat Transfer Textbook, Phlogiston Press, Cambridge, MA, USA, 2002.
[16] N.E. Bergan, Testing of the Molten Salt Electric Experiment Solar Central Receiver in an External Configuration, Sandia National Laboratories Report SAND86-8010, October 1986.